Convolutional Neural Networks and Image Patches for Lithological Classification of Brazilian Pre-Salt Rocks

Mateus Roder[2], Leandro Aparecido Passos[1], Clayton Pereira[1], João Paulo Papa[1], Altanir Flores de Mello Junior[3], Marcelo Fagundes de Rezende[3], Yaro Moisés Parizek Silva[3] and Alexandre Vidal[2]

[1]*Department of Computing, São Paulo State University (UNESP), Brazil*

[2]*Institute of Geosciences, Campinas State University (UNICAMP), Brazil*

[3]*Research Center, Leopoldo Américo Miguez de Mello Research, Development and Innovation Center (Cenpes), Brazil*

Keywords: Lithological Classification, Pre-Salt Rocks, Convolutional Neural Networks.

Abstract: Lithological classification is a process employed to recognize and interpret distinct structures of rocks, providing essential information regarding their petrophysical, morphological, textural, and geological aspects. The process is particularly interesting regarding carbonate sedimentary rocks in the context of petroleum basins since such rocks can store large quantities of natural gas and oil. Thus, their features are intrinsically correlated with the production potential of an oil reservoir. This paper proposes an automatic pipeline for the lithological classification of carbonate rocks into seven distinct classes, comparing nine state-of-the-art deep learning architectures. As far as we know, this is the largest study in the field. Experiments were performed over a private dataset obtained from a Brazilian petroleum company, showing that MobileNetV3large is the more suitable approach for the undertaking.

1 INTRODUCTION

In recent years, a more profound petrographic comprehension of rock types within petroleum basins has emerged as a crucial tool for enhancing data refinement in engineering and geology. This understanding aids in optimizing the efficient extraction of this significant fossil fuel. Moreover, lithology identification offers invaluable insights into the petrophysical characteristics of oil and gas reservoirs, including porosity and permeability. (Xu et al., 2021; Faria et al., 2022).

The analysis of rock and slide images from thin section play a pivotal role in various geoscience applications. This analysis yields precise insights into mineral composition and porosity, facilitates the identification of elements affecting fluid dynamics, enables the estimation of reservoir quality, and enhancing lithological identification (Xu et al., 2022).

As the accurate classification of rock samples is pivotal in this field, the academic community has been diligently developing tools to streamline the automated classification of thin section microscopy images. These tools often integrate machine learning and deep learning algorithms, harnessing the power of computer vision for tasks such as rock thin section classification (Polat et al., 2021; Xu et al., 2021; Faria et al., 2022).

In this context, Ghiasi-Freez et al. (Ghiasi-Freez et al., 2014) proposed an artificial neural network (ANN) to classify carbonate rocks into grainstone, wackestone, mudstone, and packstone, while Młynarczuk et al. (Młynarczuk et al., 2013) employed traditional machine learning techniques to perform classification over nine types of rocks. More recent works used deep learning architectures for the task, de Lima et al. (de Lima et al., 2019), for instance, employed convolutional neural networks (CNNs) to identify microfacies, while Nanjo et al. (Nanjo and Tanaka, 2019) applied a similar procedure to identify different lithologies in carbonate rocks. Further applications involving deep architectures for rock type classification are addressed in (Cheng and Guo, 2017; Faria et al., 2022; Xu et al., 2021).

This paper proposes a comparison of nine deep architectures for the task of carbonate rocks lithology classification into seven distinct classes, namely

Roder, M., Passos, L., Pereira, C., Papa, J., Mello Junior, A., Fagundes de Rezende, M., Silva, Y. and Vidal, A.
Convolutional Neural Networks and Image Patches for Lithological Classification of Brazilian Pre-Salt Rocks.
DOI: 10.5220/0012429100003660

In *Proceedings of the 19th International Joint Conference on Computer Vision, Imaging and Computer Graphics Theory and Applications (VISIGRAPP 2024) - Volume 3: VISAPP*, pages 648-655
ISBN: 978-989-758-679-8; ISSN: 2184-4321

Clay Spherulite, Spherulite, Grainstone, Dolomite, Arborescent Stromatolite, Laminite, Rudstone. Experiments were conducted over a private dataset of petrographic thin section images of carbonate rocks extracted over two oil wells by a Brazilian petroleum company. The main contributions of this paper are three-fold:

- to evaluate nine deep architectures in the context of carbonate rocks classification;
- to scrutinize the quality of the oil reservoirs based on the features observed on carbonate rocks that compose the well basin;
- to foster the literature regarding oil reservoir quality assessment based on carbonate rocks' classification.

The remainder of this paper is organized as follows. Section 2 provides a theoretical background regarding CNNs and Pre-Salt Carbonate Rocks, while Section 3 introduces the reader to the methods employed in this research. Further, Section 4 comprises the results and discussions. Finally, Section 5 states conclusions.

2 THEORETICAL BACKGROUND AND RELATED WORKS

In this section, we present the main concepts of convolutional neural networks, and the lithographic rock classification problem, as well as the main works related to this research.

2.1 Convolutional Neural Networks

Convolutional Neural Networks (LeCun et al., 1998) have achieved exceptional popularity in the early 2010s, becoming fundamental for solving problems related to image processing, such as image classification (Sandler et al., 2018) and segmentation (Zoph et al., 2020). As the name suggests, the main difference from the standard deep neural networks relies on the neurons, convolutional-based ones, which compose the basic blocks of CNNs, i.e., kernels responsible for performing convolution operations. By applying a convolution kernel to the data, this operation generates a new set of matrices, which are used as input data for the subsequent model layers. In signal processing, convolution is described as multiplying two signals to generate a third (Oppenheim et al., 2001).

CNNs were proposed with a base sequence of operations i.e., convolutions, application of the activation function to their output, and, optionally, sampling (pooling) (LeCun et al., 2010). As mentioned earlier, the convolution represents the matrix multiplication of the data window and a kernel. Subsequently, the transformed data pass through an activation function, whose options are numerous, such as sigmoid, hyperbolic tangent, and ReLu, for instance. In this step, the linearity is broken, and naturally, the reduction of the data dimension can occur.

Finally, the process can be followed by the output dimension reduction via the pooling layer, usually choosing a window smaller than the kernel dimension. In this step, most applications use sampling similar to a high-pass filter, letting only the maximum values of each window pass (max-pooling). The previously described steps and the learning process on a CNN were discussed extensively by Yamashita et al. (Yamashita et al., 2018). As the problems in computer vision become more challenger, many convolutional architectures variants emerged in the last decade, highlighting the residual-based CNN (ResNet) (He et al., 2016) and the MobileNet (Sandler et al., 2018).

2.2 Pre-Salt Carbonate Rock

Carbonate sedimentary rocks, formed by minerals like dolomite and calcite, denote a particularly appealing type of sediment whose features are intrinsically correlated with the production potential of an oil reservoir (Nanjo and Tanaka, 2019). Such a relationship regards the sediment composition and structure, which are especially attractive due to their capacity to store large quantities of natural gas and oil inside them (Worden et al., 2018).

The interpretation of carbonate rocks' structure may provide petrophysical, morphological, textural, and geological aspects, like framework and diagenetic composition, porous structure, and mineral distribution, among others, which contribute with valuable information about the quality of the reservoirs (Gu et al., 2018; Rabbani et al., 2017). However, interpreting such structures poses a complex problem due to the deposition process, which entails internal diagenetic modifications in their structures (Burchette, 2012), thus demanding a detailed carbonate facies' analysis for the identification of such aspects (Faria et al., 2022).

In this context, carbonate lithology performs an essential role, influencing the analysis of the reservoir characteristics and geological modelling (Duan et al., 2020), as well as providing imperative information regarding oil and gas petrographic features such as the permeability and porosity of the reservoirs (Alzubaidi et al., 2021).

3 METHODOLOGY

In this section, we present an overall description of the dataset and the experimental setup regarding the proposed approach, with hyperparameters details.

3.1 Dataset

For this study, we used 62 private petrographic thin section ("slide") images of carbonate rocks, employing the automated mineralogical mapping (QEMSCAN) technique. Out of these images, 18 originated from samples extracted from oil well "A" (ranging in depth from 5,026.05m to 5,091.65m), while the remaining 44 was sourced from oil well "B" (with depths spanning from 5,354.00m to 5,894.00m). In Figure 1, one can observe an illustrative sample slide. The QEMSCAN method, an abbreviation for Quantitative Evaluation of Minerals by Scanning Electron Microscopy, is akin to a traditional scanning electron microscope coupled with EDS (Energy Dispersive Spectroscopy) detectors; However, it operates in an automated manner, transforming chemical data into mineralogy.

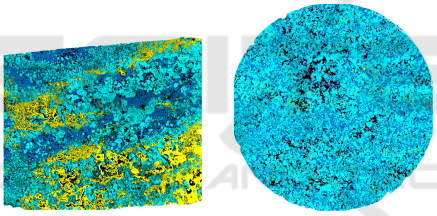

(a) (b)

Figure 1: Rock thin section from (a) oil well "A" and (b) oil well "B".

The dataset was curated by geological specialists, in which the mineral's composition and distribution were deeply investigated, resulting in seven classes for the sampled thin sections. Those classes are as follows: Clay Spherulite (0), Spherulite (1), Grainstone (2), Dolomite (3), Arborescent Stromatolite (4), Laminite (5), and Rudstone (6), with the number in brackets representing the numerical equivalence of its class. Table 1 shows the number of samples regarding each class on the dataset, and its corresponding proportion. Therefore, one can see the class imbalance on the dataset, depicting a challenge.

Regarding the image properties, the thin sections obtained with the QEMSCAN have not a standard resolution, i.e., some images have $\approx 2,500 \times 2,000$ pixels, while other ones have $\approx 2,000 \times 2,500$ pixels, or the region of interest is a small circumference inside the overall image. These facts depict a significant difficulty, requiring some pre-processing steps before the CNNs receive the data. In such a manner, a manual crop was employed to remove large blank regions, as depicted in Figure 2, marked as the centering step.

Table 1: Class proportion over the dataset.

Class	#Samples	Proportion
Clay Spherulite	9	15%
Spherulite	8	14%
Grainstone	17	29%
Dolomite	4	7%
Arborescent Stromatolite	11	19%
Laminite	4	7%
Rudstone	6	10%
Total	59	100%

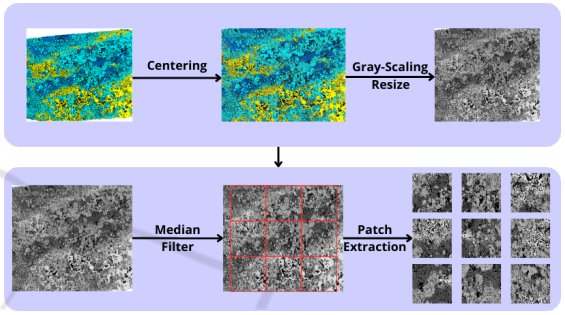

Figure 2: Pre-processing pipeline for generating the rock patches.

Following the pre-processing pipeline in Figure 2, the thin sections are converted into grayscale. Additionally, we apply the median filter with a kernel size of 3 pixels on the neighborhood to smooth the pixel intensity and reduce the noise introduced by previous conversions. The next step represents the division of each image into several patches with different patch sizes. Regarding such division, we employed three patch sizes: 250×250, 200×200, and 150×150, with a stride of 200, 150, and 100, respectively. Moreover, it is important to highlight that such sizes facilitate the resize operation to feed the images to CNN models since they have specific input dimensions (covered in the next subsection).

3.2 CNN Models

The study comprises the fine-tuning of different CNN architectures regarding the problem of rock image thin section classification. Additionally, it covers comprehension of the patch size influence on the networking processing and accuracy. Four main architectures were selected to study the patch size effect on their performance and to discover the architecture variation more suitable to the problem. The CNNs chosen were: ResNet (18, 34, 50, 101) (He et al.,

2016), DenseNet (121, 161) (Huang et al., 2017), MobileNet V3 (small and large) (Howard et al., 2019), ShuffleNet V2 (Ma et al., 2018). It is important to cite that all models employed in this study were pre-trained on the ImageNet dataset (Deng et al., 2009), which comprises more than 14 million samples, and $1,000$ classes.

In short, the ResNet (He et al., 2016) is an architecture known for its remarkable performance in image classification and computer vision tasks. The main innovation of ResNet is the use of residual blocks, also called skip connections or shortcut connections. These blocks allow the network to skip one or more layers and pass information from one layer to another, which helps mitigate the vanishing gradient problem. Such a procedure enables us to train very deep neural networks ranging from 18 to more than 100 layers, which was challenging before ResNet.

The DenseNet (Huang et al., 2017), or Densely Connected Convolutional Network, is a ResNet variant introduced to address challenges associated with training very deep networks for image classification and other computer vision tasks. The distinctive feature of DenseNet is its dense connectivity pattern. In traditional CNNs, each layer is connected only to the previous layer and the input; however, the DenseNet establishes direct connections between each layer and all subsequent layers in a feedforward manner. This dense connectivity promotes feature reuse and facilitates the flow of gradients throughout the network, which enables the training of up to 121 or 161 layers.

On the other hand, the MobileNet V3 (Howard et al., 2019) is a lightweight deep neural network architecture designed for mobile and edge devices and is an evolution of the original MobileNet V2 (Sandler et al., 2018). It introduces the concept of inverted residuals with linear bottlenecks, representing the use of lightweight depthwise separable convolutions with a shortcut connection, similar to ResNets. The width multiplier and resolution multiplier allow users to customize the model size, which names the model in small or large, according to the setup. It has demonstrated competitive performance on various benchmark datasets while being significantly smaller in size compared to larger architectures designed for cloud-based scenarios.

ShuffleNet V2 (Ma et al., 2018) is an extension of the original ShuffleNet, and it is designed to provide efficient channel shuffling and further improve the performance of deep neural networks while maintaining computational efficiency. The main innovation of ShuffleNet V2 concerns its channel shuffling operations, which help in exchanging information across channels, allowing for efficient use of feature maps. Its basic building block is the ShuffleNet unit, which consists of pointwise group convolution, channel shuffle, depthwise convolution, and another pointwise group convolution. This unit allows for efficient information exchange across channels.

3.3 Experimental Setup

Considering the CNNs input dimension limitation of 224×224 pixels and three channels (RGB), we resized the image patches, i.e., the 250, 200, and the 150, to this shape. Additionally, since the pre-trained models require three channels, and the grayscale patches have one channel, we replicated it to form the correct input shape, i.e., $224 \times 224 \times 3$. In such a manner, each CNN model was trained independently for 10 times to alleviate the stochastic behavior of parameters initialization and update.

Regarding the model's fine-tuning, we froze all the convolution layers and fine-tuned the model's final fully-connected layer (FC), appending another FC with shape $1,000 \times 7$. We fine-tuned the models' FC with Adam (Kingma and Ba, 2015) optimizer, considering a learning rate of 1×10^{-4}, and the appended FC also with Adam and a learning rate of 1×10^{-3}, for 10 epochs, with the cross-entropy loss. The batch size was 32 samples, and a Dropout layer with a probability of 10% of neurons being dropped on the FC layer from the model was employed. Such hyperparameters were empirically defined using the validation set (forward covered).

Additionally, one can define the data split employed in the experimental setup. This step stands for a hold-out split with 85% of data to train, and 15% to test, being 15% of the train set employed as the validation set. Since the dataset is highly imbalanced (Table 1), we opted to stratify the hold-out procedure by the class, keeping the class proportion on the partitions (train, validation, and test). Furthermore, it is meaningful to highlight that, by changing the patch size, the amount of data available to the partitions varies since we fixed the proportions instead of the number of samples, which can generate more patches when the patch size is reduced, for instance.

We employed four classical evaluation measures, Precision, Recall, F1-score, and Accuracy, to evaluate the models' performance. Such measures depict a standard evaluation approach for classification problems. Finally, to run the defined combinations of experiments, we utilized an Intel Xeon with 32 cores, 128Gb of RAM, and a GTX TITAN X GPU with 12Gb of memory. Unfortunately, even though this GPU enables us to run different models, more complex ones or more samples on the batch were not pos-

Table 2: Performance evaluation regarding the patches with size 250.

		Precision	Recall	F1	Accuracy
ResNet18	mean	0.5811	0.5673	0.5651	0.5673
	std	0.0196	0.0245	0.0244	0.0245
ResNet34	mean	0.5912	0.5820	0.5785	0.5820
	std	0.0304	0.0303	0.0293	0.0303
ResNet50	mean	0.6165	0.6034	0.5965	0.6034
	std	0.0164	0.0176	0.0180	0.0176
ResNet101	mean	0.6410	0.6212	0.6160	0.6212
	std	0.0281	0.0283	0.0286	0.0283
DenseNet121	mean	0.6447	0.6320	0.6263	0.6320
	std	0.0214	0.0250	0.0254	0.0250
DenseNet161	mean	0.6658	0.6591	0.6561	0.6591
	std	0.0133	0.0131	0.0144	0.0131
MobileNetV3small	mean	0.6337	0.6185	0.6167	0.6185
	std	0.0237	0.0108	0.0114	0.0108
MobileNetV3large	mean	**0.6974**	**0.6889**	**0.6869**	**0.6889**
	std	0.0182	0.0192	0.0205	0.0192
ShuffleNetV2	mean	0.6429	0.6327	0.6285	0.6327
	std	0.0123	0.0128	0.0148	0.0128

sible due to the GPU memory consumption.

4 EXPERIMENTAL RESULTS

Regarding the experimental results, Tables 2, 3, and 4 present the mean and standard deviation for the test set partition of the four evaluated metrics obtained from ten independent repetitions, considering the three patch sizes selected over all CNN models. Additionally, best results are marked in bold.

From Table 2, one can observe the performance improvement over the precision, recall, F1-score, and accuracy for the ResNet models, which represents that, by increasing the number of residual blocks, the model learns more about the data and generalizes better. Such scalability stands for almost 2% in accuracy, starting with ResNet18 with 0.5673 to 0.5820 on ResNet34, for instance. Analyzing the DenseNet, we observed the same behavior from DenseNet121 to DenseNet161, in which all measures were improved with more dense blocks being employed, i.e., 121 versus 161. However, the performance improvement over the previous models was not as accentuated as the improvement from the MobileNet V3 small to the large, with the larger model achieving a mean accuracy of 0.6889, an impressive result over all models, even the ShuffleNet V2 (0.6327).

Regarding Table 3, one can perceive the same behavior previously observed, i.e., as the model complexity increases, the performance measures increase within the same model family. However, one can see the ResNet101 surpassing both DenseNets in precision, recall, F1-score, and accuracy, which indicates that a "simpler" model can benefit more than "complex" models when more data is available, since reducing the patch size the number of samples increases. Moreover, as expected, the MobileNet V3 large achieved better performance overall measures and other models, while the ResNet101 ranked in second place.

Table 3: Performance evaluation regarding the patches with size 200.

		Precision	Recall	F1	Accuracy
ResNet18	mean	0.6465	0.6337	0.6296	0.6337
	std	0.0208	0.0173	0.0178	0.0173
ResNet34	mean	0.6573	0.6420	0.6384	0.6420
	std	0.0260	0.0278	0.0294	0.0278
ResNet50	mean	0.6921	0.6658	0.6621	0.6658
	std	0.0178	0.0287	0.0317	0.0287
ResNet101	mean	0.7115	0.6963	0.6948	0.6963
	std	0.0161	0.0203	0.0193	0.0203
DenseNet121	mean	0.6760	0.6599	0.6577	0.6599
	std	0.0234	0.0189	0.0195	0.0189
DenseNet161	mean	0.6868	0.6777	0.6736	0.6777
	std	0.0147	0.0133	0.014	0.0133
MobileNetV3small	mean	0.6521	0.6460	0.6429	0.6460
	std	0.0111	0.0146	0.0142	0.0146
MobileNetV3large	mean	**0.7194**	**0.7125**	**0.7105**	**0.7125**
	std	0.0174	0.0170	0.0179	0.0170
ShuffleNetV2	mean	0.6496	0.6401	0.6391	0.6401
	std	0.0209	0.0219	0.0219	0.0219

Table 4: Performance evaluation regarding the patches with size 150.

		Precision	Recall	F1	Accuracy
ResNet18	mean	0.6575	0.6462	0.6442	0.6462
	std	0.0096	0.0147	0.0134	0.0147
ResNet34	mean	0.6465	0.6372	0.6355	0.6372
	std	0.0163	0.0177	0.0197	0.0177
ResNet50	mean	0.6927	0.6752	0.6722	0.6752
	std	0.0149	0.0168	0.0166	0.0168
ResNet101	mean	0.7166	0.7081	0.7052	0.7081
	std	0.0140	0.0157	0.0165	0.0157
DenseNet121	mean	0.6762	0.6643	0.6599	0.6643
	std	0.0136	0.0169	0.0173	0.0169
DenseNet161	mean	0.6993	0.6921	0.6892	0.6921
	std	0.0142	0.0129	0.0136	0.0129
MobileNetV3small	mean	0.6649	0.6578	0.6564	0.6578
	std	0.0124	0.0101	0.0100	0.0101
MobileNetV3large	mean	**0.7282**	**0.7237**	**0.7222**	**0.7237**
	std	0.0085	0.0091	0.0084	0.0091
ShuffleNetV2	mean	0.6263	0.6159	0.6130	0.6159
	std	0.0088	0.0098	0.0115	0.0098

Regarding Table 4, the behavior observed in Tables 3 and 2 slightly changed, i.e., the ResNet34 did not improve its performance as expected and observed on patches 250 and 200. However, once more, the ResNet101 surpasses both DenseNets in precision, recall, F1-score, and accuracy, with all measures greater than 0.70. Once again, the MobileNet V3 large achieved better performance over all measures (greater than 0.72) and models, while the ResNet101 also ranked in second place. Finally, the ShuffleNet V2 achieved the worst performance in all measures, which is interesting since the model was not the worst on previous patch sizes.

In summary, one can elucidate some key findings. Firstly, the residual models achieved good performance in all measures, highlighting the ResNet101, which represents a good alternative for the pre-salt

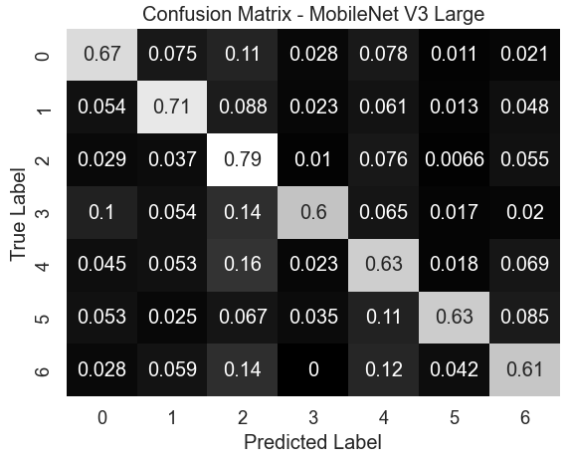

Figure 3: Confusion matrix for MobileNet V3 Large and patch size of 250.

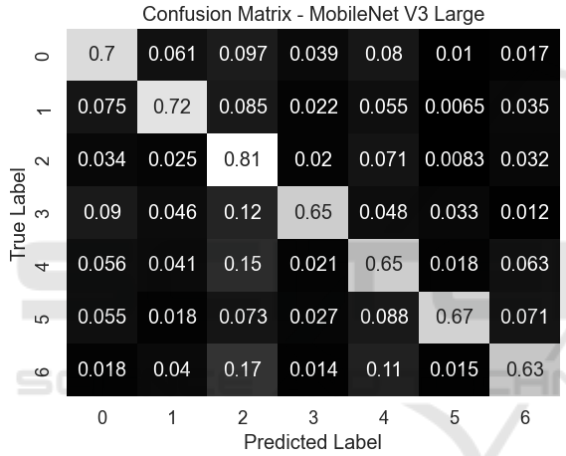

Figure 4: Confusion matrix for MobileNet V3 Large and patch size of 200.

rock classification problem, especially if more data is available to fine-tune. The second finding is that MobileNet V3 large is more suitable to our problem, even with low data volume, since its results surpassed all models for the three patch sizes employed. Moreover, a patch size of 150 seems to be a good alternative, however, mainly when more data is available. As complementary results, the confusion matrices averaged over the 10 repetitions, in percentage, for the best model overall (MobileNet V3 large) are presented in Figures 3, 4, and 5.

Finally, comparing Figures 3, 4, and 5, one can see the performance improvement on the main diagonal, from the 250 to 150 patch sizes. First, from Figure 3, the greater error percentage classification stands for predicting as class 2 the patches of class 4, i.e., 16% of the test samples. Such an observation represents a possible bias since class 2 has more data on the

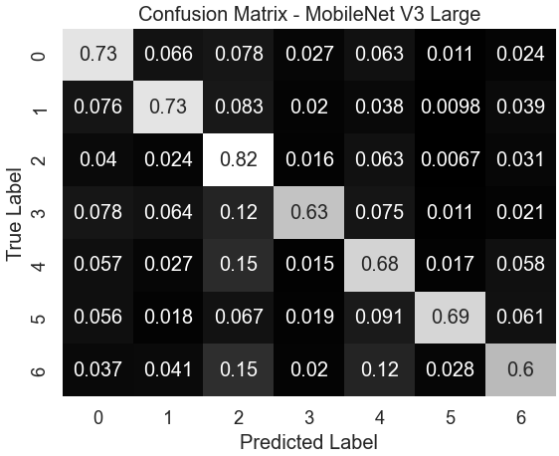

Figure 5: Confusion matrix for MobileNet V3 Large and patch size of 150.

dataset. Regarding Figure 4, the same behavior occurred, i.e., more samples have been classified incorrectly as class 2 (column 2). Additionally, the main diagonal increased its values. Lastly, Figure 5 gathers the better result, with a substantial increase on the main diagonal, and a reduction in samples incorrectly classified as class 2 (column 2).

5 CONCLUSIONS

In this paper, we addressed the problem of pre-salt rock lithology classification with convolutional neural networks. In such a manner, the study objective was to understand the learning and generalization capability of state-of-the-art pre-trained models employed in a fine-tuning phase with low data availability and high-class imbalance. Additionally, we extended our investigation on the patch size used to crop the original image thin section.

We employed a total of nine models, from ResNets to MobileNets, trained on three different patch sizes, 250, 200, and 150 pixels crop. The first patch size leads us to deep models with all performance measures greater than 0.56 percentage mean, highlighting the MobileNet V3 large, with a mean greater than 0.68, representing a good starting point, since the dataset has only 59 thin sections.

Regarding the second and third patch sizes (200 and 150), we observed patterns in the models' behavior, i.e., with more data available to train, the performance increases for most of the employed models, with the better one being the MobileNet V3 large so far. Additionally, even with a small crop, 150 pixels, the resizing operation does not negatively interfere. Regarding the best MobileNet, its superior per-

formance indicates the model is a good candidate to be deployed as we have more data collected to improve the training.

Even with the promising results using image patches to feed the architectures, it represents a challenge if we want to modify the patch size on a substantial scale, such as 500 or 50 pixels since the pretrained architectures have fixed input sizes. We expect to explore this challenge by modifying the first layer and resizing its output to match the original configuration, considering more data to train the required lower-level layers.

Considering future works, we aim to deeply investigate modifications to the MobileNet architecture to improve our results, and aggregate multimodal data. Additionally, we expect to collect more data to train models from scratch and compare it with its fine-tuned version.

ACKNOWLEDGEMENTS

The authors are grateful to Petrobras-CENPES, Brazil, for providing the oil well images and grant #5472. Also, we are grateful to Fundação de Amparo à Pesquisa do Estado de São Paulo (FAPESP), Brazil grants #2023/10823 – 6, for their financial support.

REFERENCES

Alzubaidi, F., Mostaghimi, P., Swietojanski, P., Clark, S. R., and Armstrong, R. T. (2021). Automated lithology classification from drill core images using convolutional neural networks. *Journal of Petroleum Science and Engineering*, 197:107933.

Burchette, T. P. (2012). Carbonate rocks and petroleum reservoirs: a geological perspective from the industry. *Geological Society, London, Special Publications*, 370(1):17–37.

Cheng, G. and Guo, W. (2017). Rock images classification by using deep convolution neural network. In *Journal of Physics: Conference Series*, volume 887, page 012089. IOP Publishing.

de Lima, R. P., Bonar, A., Coronado, D. D., Marfurt, K., and Nicholson, C. (2019). Deep convolutional neural networks as a geological image classification tool. *The Sedimentary Record*, 17(2):4–9.

Deng, J., Dong, W., Socher, R., Li, L.-J., Li, K., and Fei-Fei, L. (2009). Imagenet: A large-scale hierarchical image database. In *2009 IEEE Conference on Computer Vision and Pattern Recognition*, pages 248–255.

Duan, Y., Xie, J., Li, B., Wang, M., Zhang, T., and Zhou, Y. (2020). Lithology identification and reservoir characteristics of the mixed siliciclastic-carbonate rocks of the lower third member of the shahejie formation in the south of the laizhouwan sag, bohai bay basin, china. *Carbonates and Evaporites*, 35:1–19.

Faria, E., Coelho, J. M., Matos, T. F., Santos, B. C., Trevizan, W. A., Gonzalez, J., Bom, C. R., de Albuquerque, M. P., and de Albuquerque, M. P. (2022). Lithology identification in carbonate thin section images of the brazilian pre-salt reservoirs by the computational vision and deep learning. *Computational Geosciences*, 26(6):1537–1547.

Ghiasi-Freez, J., Honarmand-Fard, S., and Ziaii, M. (2014). The automated dunham classification of carbonate rocks through image processing and an intelligent model. *Petroleum science and technology*, 32(1):100–107.

Gu, Y., Bao, Z., and Rui, Z. (2018). Prediction of shell content from thin sections using hybrid image process techniques. *Journal of Petroleum Science and Engineering*, 163:45–57.

He, K., Zhang, X., Ren, S., and Sun, J. (2016). Deep residual learning for image recognition. In *Proceedings of the IEEE conference on computer vision and pattern recognition*, pages 770–778.

Howard, A., Sandler, M., Chu, G., Chen, L.-C., Chen, B., Tan, M., Wang, W., Zhu, Y., Pang, R., Vasudevan, V., et al. (2019). Searching for mobilenetv3. In *Proceedings of the IEEE/CVF international conference on computer vision*, pages 1314–1324.

Huang, G., Liu, Z., Van Der Maaten, L., and Weinberger, K. Q. (2017). Densely connected convolutional networks. In *Proceedings of the IEEE conference on computer vision and pattern recognition*, pages 4700–4708.

Kingma, D. P. and Ba, J. (2015). Adam: A method for stochastic optimization. In *3rd International Conference on Learning Representations, ICLR*.

LeCun, Y., Bottou, L., Bengio, Y., Haffner, P., et al. (1998). Gradient-based learning applied to document recognition. *Proceedings of the IEEE*, 86(11):2278–2324.

LeCun, Y., Kavukcuoglu, K., and Farabet, C. (2010). Convolutional networks and applications in vision. In *Proceedings of 2010 IEEE International Symposium on Circuits and Systems*, pages 253–256.

Ma, N., Zhang, X., Zheng, H.-T., and Sun, J. (2018). Shufflenet v2: Practical guidelines for efficient cnn architecture design. In *Proceedings of the European Conference on Computer Vision (ECCV)*.

Młynarczuk, M., Górszczyk, A., and Ślipek, B. (2013). The application of pattern recognition in the automatic classification of microscopic rock images. *Computers & Geosciences*, 60:126–133.

Nanjo, T. and Tanaka, S. (2019). Carbonate lithology identification with machine learning. In *Abu Dhabi International Petroleum Exhibition and Conference*, page D021S060R001. SPE.

Oppenheim, A. V., Buck, J. R., and Schafer, R. W. (2001). *Discrete-time signal processing. Vol. 2*. Upper Saddle River, NJ: Prentice Hall.

Polat, Ö., Polat, A., and Ekici, T. (2021). Automatic classification of volcanic rocks from thin section images

using transfer learning networks. *Neural Computing and Applications*, 33(18):11531–11540.

Rabbani, A., Assadi, A., Kharrat, R., Dashti, N., and Ayatollahi, S. (2017). Estimation of carbonates permeability using pore network parameters extracted from thin section images and comparison with experimental data. *Journal of Natural Gas Science and Engineering*, 42:85–98.

Sandler, M., Howard, A., Zhu, M., Zhmoginov, A., and Chen, L.-C. (2018). Mobilenetv2: Inverted residuals and linear bottlenecks. In *Proceedings of the IEEE conference on computer vision and pattern recognition*, pages 4510–4520.

Worden, R., Armitage, P., Butcher, A., Churchill, J., Csoma, A., Hollis, C., Lander, R., and Omma, J. (2018). Petroleum reservoir quality prediction: overview and contrasting approaches from sandstone and carbonate communities. *Geological Society, London, Special Publications*, 435(1):1–31.

Xu, Z., Ma, W., Lin, P., and Hua, Y. (2022). Deep learning of rock microscopic images for intelligent lithology identification: Neural network comparison and selection. *Journal of Rock Mechanics and Geotechnical Engineering*, 14(4):1140–1152.

Xu, Z., Ma, W., Lin, P., Shi, H., Pan, D., and Liu, T. (2021). Deep learning of rock images for intelligent lithology identification. *Computers & Geosciences*, 154:104799.

Yamashita, R., Nishio, M., Do, R. K. G., and Togashi, K. (2018). Convolutional neural networks: an overview and application in radiology. *Insights into imaging*, 9(4):611–629.

Zoph, B., Ghiasi, G., Lin, T.-Y., Cui, Y., Liu, H., Cubuk, E. D., and Le, Q. V. (2020). Rethinking pre-training and self-training. *arXiv preprint arXiv:2006.06882*.